GIRK currents in VTA dopamine neurons control the sensitivity of mice to cocaine-induced locomotor sensitization

Robert A. Rifkin[a,b,c,d], Deborah Huyghe[e], Xiaofan Li[a,b], Manasa Parakala[e], Erin Aisenberg[a,b], Stephen J. Moss[e], and Paul A. Slesinger[a,b,c,1]

[a]Department of Neuroscience, Icahn School of Medicine at Mount Sinai, New York, NY 10029; [b]Friedman Brain Institute, Icahn School of Medicine at Mount Sinai, New York, NY 10029; [c]Graduate Program in Biomedical Science, Icahn School of Medicine at Mount Sinai, New York, NY 10029; [d]Medical Scientist Training Program, Icahn School of Medicine at Mount Sinai, New York, NY 10029; and [e]Department of Neuroscience, Tufts University School of Medicine, Boston, MA 02155

Edited by Lily Yeh Jan, University of California, San Francisco, CA, and approved August 21, 2018 (received for review May 7, 2018)

$GABA_BR$-dependent activation of G protein-gated inwardly rectifying potassium channels (GIRK or $K_{IR}3$) provides a well-known source of inhibition in the brain, but the details on how this important inhibitory pathway affects neural circuits are lacking. We used sorting nexin 27 (SNX27), an endosomal adaptor protein that associates with GIRK2c and GIRK3 subunits, to probe the role of GIRK channels in reward circuits. A conditional knockout of SNX27 in both substantia nigra pars compacta and ventral tegmental area (VTA) dopamine neurons leads to markedly smaller $GABA_BR$- and dopamine D_2R-activated GIRK currents, as well as to suprasensitivity to cocaine-induced locomotor sensitization. Expression of the SNX27-insensitive GIRK2a subunit in SNX27-deficient VTA dopamine neurons restored GIRK currents and $GABA_BR$-dependent inhibition of spike firing, while also resetting the mouse's sensitivity to cocaine-dependent sensitization. These results establish a link between slow inhibition mediated by GIRK channels in VTA dopamine neurons and cocaine addiction, revealing a therapeutic target for treating addiction.

psychostimulants | addiction | potassium channel | dopamine | ventral tegmental area

A majority of dopamine (DA) in the brain is produced by DA neurons in two small, adjacent nuclei in the midbrain: the ventral tegmental area (VTA) and the substantia nigra pars compacta (SNc). VTA DA neurons project to the nucleus accumbens (NAc), medial prefrontal cortex (mPFC), and other regions, and are strongly associated with learning, reward, and addiction (1). SNc DA neurons, on the other hand, project predominantly to the dorsal striatum (DS) and are traditionally associated with the initiation of motor behaviors, a process that is disrupted in Parkinson disease. Addictive drugs converge on a common pathway of elevating DA levels in the NAc (2), mPFC (3), and VTA (4). These increases in DA concentration contribute to the neuronal plasticity that leads to compulsive substance use despite negative consequences (5, 6). Consistent with this role, direct optogenetic excitation of VTA DA neurons can induce conditioned place preference, similar to that with drugs of abuse (7). Additionally, mice will perform intracranial self-stimulation via optogenetic excitation of VTA DA neurons (8). Together, these and other studies (1) implicate the activity of VTA DA neurons in rewarding and addictive behaviors.

Classically, DA neurons in the midbrain were defined by the presence of a hyperpolarization-activated cyclic nucleotide-gated channel-mediated current (I_h); cells lacking this current were assumed to be GABAergic (9). Howewver, several recent studies suggest that the population of DA neurons is more diverse, and includes I_h^- neurons (10). VTA DA neurons expressing I_h project primarily to the NAc lateral shell, while DA neurons lacking I_h project to the NAc core and medial shell, mPFC, and amygdala (11). Interestingly, these populations are differentially modulated by cocaine (12). SNc DA neurons also express I_h and have been recently shown to have similar functions to VTA DA neurons in reward and addiction (13, 14). Thus, SNc DA neurons may play an important but largely uncharacterized role in addictive behavior. Because drugs of abuse can have markedly different effects on different cell populations (12, 15), and changes in neuronal circuitry determine the behavioral response to drugs of abuse (5, 6), it is important to specifically interrogate these neuronal populations, using cell type- and projection-specific techniques.

An important pathway for regulating neuronal excitability in VTA DA and SNc DA neurons is provided by G protein-gated inwardly rectifying potassium (GIRK or $K_{IR}3$) channels (16). GIRK channels are activated by $G\beta\gamma$ subunits (17–19) of $G\alpha_{i/o}$-type heterotrimeric G proteins that couple to metabotropic neurotransmitter receptors, such as the γ-amino butyric acid (GABA) type B ($GABA_B$) (20) and dopamine type 2 (D_2) (21) receptors. Activation of these receptors leads to opening of GIRK channels, producing an outward K^+ current that hyperpolarizes the cell's membrane potential and inhibits neuronal action potential firing. GIRK channels have been shown to be critical regulators of VTA and SNc DA neuronal activity in the context of addiction (1). Exposure to cocaine or methamphetamine (22–25) leads to down-regulation of agonist-evoked $GABA_BR$-GIRK currents in VTA DA neurons via a mechanism

Significance

Activation of G protein-gated inwardly rectifying potassium (GIRK) channels inhibits neuronal activity in the brain, but details are lacking on how this important pathway influences neural circuits in the reward pathway. Here, we provide an example of where control of trafficking of GIRK channels by a cytoplasmic protein, sorting nexin 27, determines the sensitivity of mice to cocaine in a model of addiction known as locomotor sensitization. These results implicate GIRK channels as a therapeutic target for treating addiction, as well as other psychiatric disorders involving dopamine dysregulation.

Author contributions: R.A.R., X.L., S.J.M., and P.A.S. designed research; R.A.R., D.H., X.L., M.P., and E.A. performed research; R.A.R. contributed new reagents/analytic tools; R.A.R. and P.A.S. analyzed data; S.J.M. supervised the team at Tufts; P.A.S. supervised the project; and R.A.R. and P.A.S. wrote the paper.

Conflict of interest statement: S.J.M serves as a consultant for SAGE Therapeutics and AstraZeneca, relationships that are regulated by Tufts University and do not impact on this study.

This article is a PNAS Direct Submission.

[1]To whom correspondence should be addressed. Email: paul.slesinger@mssm.edu.

This article contains supporting information online at www.pnas.org/lookup/suppl/doi:10.1073/pnas.1807788115/-/DCSupplemental.

Published online September 18, 2018.

that requires the GIRK3 subunit (25) and intracellular Ca^{2+} (24). Selective deletion of GIRK2 from DA neurons results in elevated cocaine-dependent locomotor sensitization and increased intravenous cocaine self-administration (26). The subcellular localization, surface expression and recycling of GIRK channels have emerged as key properties governing their functional role in vivo (16, 27), but the mechanism controlling trafficking of GIRK channels remains poorly understood.

Attempts to understand the trafficking of GIRK channels led to the identification of sorting nexin 27 (SNX27) as a cytoplasmic protein that binds to and regulates GIRK channels containing PDZ-binding motifs (28). SNX27 is an adaptor protein that contains a PDZ domain, Phox homology (PX) domain, and 4.1/ezrin/radixin/moesin (FERM)-like domain (29, 30), and is itself regulated by psychostimulants (30). In mice lacking SNX27 in DA neurons ($SNX27_{DA}$ KO), $GABA_BR$-activated GIRK currents are significantly smaller in VTA DA neurons, resulting in an elevated locomotor response to a single injection of cocaine (31). A potential susceptibility of $SNX27_{DA}$ KO mice to becoming addicted to psychostimulants, such as in a locomotor sensitization test, however, is unknown. Furthermore, the role of SNX27 in regulating GIRK channels in specific DA neuron subpopulations, such as VTA DA neurons projecting to the NAc or SNc DA neurons projecting to the DS, has not been investigated. In the present study, we determined that SNX27 is important for maintaining GIRK currents in both VTA DA and SNc DA neurons, and that reduction of GIRK currents in VTA DA neurons enhances the locomotor-sensitizing effects of cocaine. These results provide a clear example of where GIRK currents in VTA DA neurons control the sensitivity of mice to cocaine in a model of addiction.

Results

SNX27 Regulates $GABA_BR$-GIRK Currents in Both VTA and SNc DA Neurons. In most neurons, GIRK1, GIRK2, and GIRK3 subunits are expressed together. In contrast, VTA DA neurons express only GIRK2c and GIRK3 subunits (15) and SNc DA neurons express only two splice variants of GIRK2, GIRK2a, and GIRK2c (32). SNX27 associates directly with a C-terminal PDZ motif (i.e., ESKV), present in GIRK2c and GIRK3 (28). Previous work established that ablation of SNX27 in VTA DA neurons leads to reduced $GABA_BR$-GIRK currents (31). It was unknown whether the loss of SNX27 affects GIRK currents in SNc DA neurons, which lack the GIRK3 subunit. To address this question, we compared the $GABA_BR$-activated GIRK currents in VTA DA and SNc DA neurons lacking SNX27, using a conditional KO strategy (*Materials and Methods*).

We recorded macroscopic currents from the VTA (*SI Appendix*, Fig. S1*A*) or SNc (*SI Appendix*, Fig. S1*D*) DA neurons in acutely prepared slices from $SNX27_{DA}$ KO and control mice (i.e., $SNX27^{fl/fl}$ and DAT-$Cre^{+/-}$). $SNX27_{DA}$ KO mice were generated by breeding $SNX27^{fl/fl}$ mice with DAT-$Cre^{+/-}$ mice, which express Cre in dopamine transporter (DAT)-containing DA neurons (31). DA neurons were identified by the presence of I_h and cell size (23, 33). No statistical differences in the amplitude of I_h current and cell membrane capacitance were detected among different genotypes (*SI Appendix*, Table S1). Bath application of a saturating concentration of baclofen (300 μM) (15) elicited the canonical desensitizing, outward current ($I_{Baclofen}$), which was blocked by the K_{IR} inhibitor Ba^{2+}. In the VTA, the amplitude of $I_{Baclofen}$ was significantly smaller in DA neurons from $SNX27_{DA}$ KO mice (*SI Appendix*, Fig. S1 *B* and *C*), similar to previous results (31). In the SNc, $I_{Baclofen}$ was also significantly smaller in DA neurons from $SNX27_{DA}$ KO mice, compared with $SNX27^{fl/fl}$ and DAT-$Cre^{+/-}$ control mice (*SI Appendix*, Fig. S1 *E* and *F*). Thus, SNX27 appears to regulate GIRK signaling in both VTA and SNc DA neurons.

SNX27 Regulates Excitability and GIRK Currents in VTA-to-NAc and SNc-to-DS Projecting DA Neurons. Recent studies have indicated that midbrain DA neurons with diverse electrophysiological phenotypes, projection targets, and behavioral effects are distributed in a medial-to-lateral pattern that spans subregions of the VTA and the SNc (10–12). We therefore sought to characterize the effect of the SNX27 KO in a DA cell type- and projection-specific manner. To identify VTA DA neurons projecting to the NAc, we injected a retrograding adeno-associated virus 5 (AAV5) that expresses Cre-dependent eYFP (AAV.DIO.eYFP) into the NAc of $SNX27_{TH}$ KO mice or TH-$Cre^{+/-}$ controls, and recorded from YFP^+ neurons in the VTA after 4–5 wk (Fig. 1*A*). We injected the NAc lateral shell, which is the primary target of "conventional" I_h^+ and D_2R-expressing DA neurons in the VTA (11). Recently, some concern has been raised for the selection of Cre-driver lines for targeting midbrain DA neurons (34, 35). Therefore, we also used a Bac-transgenic TH-$Cre^{+/-}$ line, backcrossed more than five generations into C57BL/6 (36, 37), to breed with $SNX27^{fl/fl}$ mice (i.e., $SNX27_{TH}$ KO). In VTA DA neurons projecting to the NAc of TH-$Cre^{+/-}$ mice, we recorded large $GABA_BR$-GIRK currents ($I_{Baclofen}$ = 195.0 ± 25.5 pA, n = 16 cells/6 mice) and D_2R-GIRK currents ($I_{Quinpirole}$ = 37.9 ± 10.0 pA, n = 7 cells/3 mice) (Fig. 1 *B–E*), consistent with previous findings in DAT-$Cre^{+/-}$ mice (*SI Appendix*, Fig. S1). Similar to $SNX27_{DA}$ KO mice, we observed significantly smaller $GABA_BR$-GIRK currents ($I_{Baclofen}$ = 79.6 ± 26.0 pA, n = 9 cells/5 mice, P = 0.0035) (see *SI Appendix*, *Supplemental Materials and Methods* for complete statistical results) and D_2R-GIRK currents ($I_{Quinpirole}$ = 7.7 ± 3.7 pA, n = 7 cells/3 mice, P = 0.0379) in VTA-to-NAc projecting DA neurons of $SNX27_{TH}$ KO mice (Fig. 1 *B–E*). Thus, two different lines of mice lacking SNX27, $SNX27_{DA}$ KO and $SNX27_{TH}$ KO, exhibit reduced GIRK currents.

In current-clamp recordings, we found that baclofen application hyperpolarized the resting membrane potential by −24.0 mV (±2.7 mV, n = 14 cells/5 mice) in VTA-to-NAc projecting DA neurons from TH-$Cre^{+/-}$ mice (Fig. 1*F*). The baclofen-evoked hyperpolarization was smaller in $SNX27_{TH}$ KO mice (ΔV_m = −11.6 ± 1.6 mV, n = 9 cells/5 mice, P = 0.0043) (Fig. 1*F*). Taken together, the electrophysiological recordings revealed reduced $GABA_BR$-dependent activation of GIRK channels. We next examined whether loss of SNX27 in midbrain DA neurons altered total protein levels of GIRK2 or $GABA_B$ receptors. In VTA/SNc midbrain micropunches, Western analysis for $GABA_B$ R1, $GABA_B$ R2, and GIRK2 showed no significant decrease in total protein (*SI Appendix*, Fig. S2), suggesting that changes in channel trafficking may underlie the decrease in GIRK current.

To identify SNc DA neurons that project to the DS, we injected AAV.DIO.eYFP into the DS of $SNX27_{TH}$ KO or TH-$Cre^{+/-}$ mice, and recorded from YFP-labeled neurons in the SNc (Fig. 1*G*). In TH-$Cre^{+/-}$ mice, SNc-to-DS projecting DA neurons express large $GABA_BR$-GIRK currents ($I_{Baclofen}$ = 414 ± 65 pA, n = 12 cells/4 mice) and D_2R-GIRK currents ($I_{Quinpirole}$ = 107 ± 39 pA, n = 9 cells/3 mice). In $SNX27_{TH}$ KO mice, there was a significant decrease in $GABA_BR$-GIRK currents ($I_{Baclofen}$ = 125.4 ± 23.2 pA, n = 9 cells/4 mice, P = 0.0003) and D_2R-GIRK currents ($I_{Quinpirole}$ = 17.6 ± 5.9 pA, n = 9 cells/4 mice, P = 0.0056) (Fig. 1 *H–K*). Similar to VTA-to-NAc DA neurons, baclofen hyperpolarized the resting membrane potential (ΔV_m = −22.3 ± 2.0 mV, n = 12 cells/4 mice) in TH-$Cre^{+/-}$ mice, but to a smaller degree in $SNX27_{TH}$ KO (ΔV_m = −15.4 ± 1.9 mV, n = 9 cells/4 mice, P = 0.0278) (Fig. 1*L*). These findings demonstrate that SNX27 is required for maintaining $GABA_BR$-GIRK and D_2R-GIRK signaling in both ventral and DS-projecting DA neurons. Furthermore, SNX27 appears to regulate $GABA_BR$-GIRK and D_2R-GIRK signaling in the absence of the GIRK3 subunit, because SNc DA neurons appear to lack GIRK3 (32).

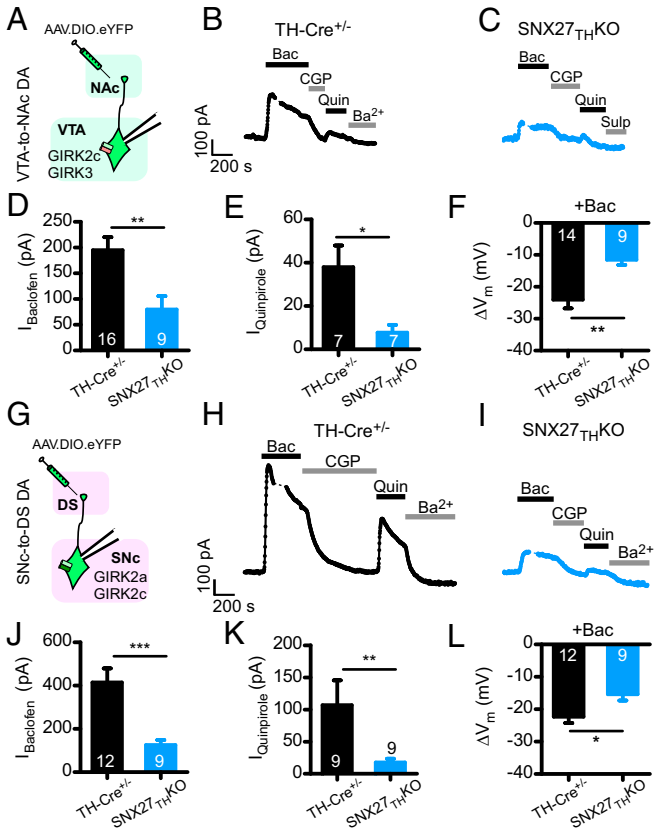

Fig. 1. Reduced $GABA_BR$-GIRK and D_2R-GIRK currents in VTA-to-NAc and SNc-to-DS projecting DA neurons in $SNX27_{TH}$ KO mice. (*A*) Cartoon shows AAV.DIO.eYFP injection into NAc and recording of labeled DA neuron in VTA. DA neurons were confirmed by the presence of I_h current (*SI Appendix*, Table S2). Representative current traces for labeled VTA DA neurons in TH-$Cre^{+/-}$ (*B*, black) and $SNX27_{TH}$ KO (*C*, blue) mice show response to bath application of (±)-baclofen (Bac, 300 μM), CGP54626 (CGP, 5 μM), (-)-quinpirole (Quin, 100 μM), (S)-(-)-sulpiride (8 μM), or Ba^{2+} (1 mM). V_h = −40 mV. Gap in current trace represents switch to current-clamp. (*D–F*) Bar graphs show mean $I_{Baclofen}$, $I_{Quinpirole}$, and baclofen-induced hyperpolarization in VTA-to-NAc DA neurons. (*D*) $I_{Baclofen}$ is significantly smaller in VTA-to-NAc DA neurons of $SNX27_{TH}$ KO mice (n = 9/5 mice) compared with TH-$Cre^{+/-}$ control (n = 16/6 mice, $^{**}P = 0.0035$). (*E*) $I_{Quinpirole}$ is significantly smaller in $SNX27_{TH}$ KO mice (n = 7/3 mice) compared with TH-$Cre^{+/-}$ controls (n = 7/3 mice, $^{*}P = 0.0379$). (*F*) Baclofen-dependent hyperpolarization of resting membrane potential (ΔV_m) is reduced in $SNX27_{TH}$ KO mice (n = 9/5 mice), compared with TH-$Cre^{+/-}$ controls (n = 14/5 mice, $^{**}P = 0.0043$). (*G*) Cartoon shows AAV.DIO.eYFP injection into DS and recording of labeled DA neuron in SNc. Current traces are shown for SNc DA neurons in TH-$Cre^{+/-}$ (*H*, black) and $SNX27_{TH}$ KO (*I*, blue) mice. (*J*) In SNc-to-DS projecting DA neurons, $I_{Baclofen}$ is smaller in $SNX27_{TH}$ KO mice (n = 9/4 mice) compared with TH-$Cre^{+/-}$ control (n = 12 cells/4 mice, $^{***}P = 0.0003$). (*K*) $I_{Quinpirole}$ is reduced in $SNX27_{TH}$ KO mice (n = 9/4 mice) compared with TH-$Cre^{+/-}$ control (n = 9/3 mice, $^{**}P = 0.0056$). (*L*) Baclofen-dependent ΔV_m is reduced in $SNX27_{TH}$ KO mice (n = 9/4 mice) compared with TH-$Cre^{+/-}$ mice (n = 12/4 mice, $^{*}P = 0.0278$). Mann–Whitney *U* test.

A reduction in $GABA_BR$-GIRK currents can increase the excitability of DA neurons (31). To examine this in VTA-to-NAc projecting DA neurons, we measured the firing rate induced by current injections of increasing amplitude (e.g., 20–300 pA) in the absence and then presence of baclofen. In TH-$Cre^{+/-}$ mice, the spike number increased with larger current injections, but was suppressed by baclofen at most current steps (interaction between drug and current, $P < 0.0001$, n = 12 cells/6 mice). Baclofen application also reduced firing in the $SNX27_{TH}$ KO mice (interaction between drug and current, $P = 0.0096$, n = 9 cells/5 mice) (Fig. 2 *A* and *B*). To directly compare the effect of baclofen on VTA-to-NAc projecting DA neurons in $SNX27_{TH}$ KO mice with those in TH-$Cre^{+/-}$ mice, we calculated the baclofen-induced reduction in firing (i.e., Δspike number). In $SNX27_{TH}$ KO mice, the Δspike

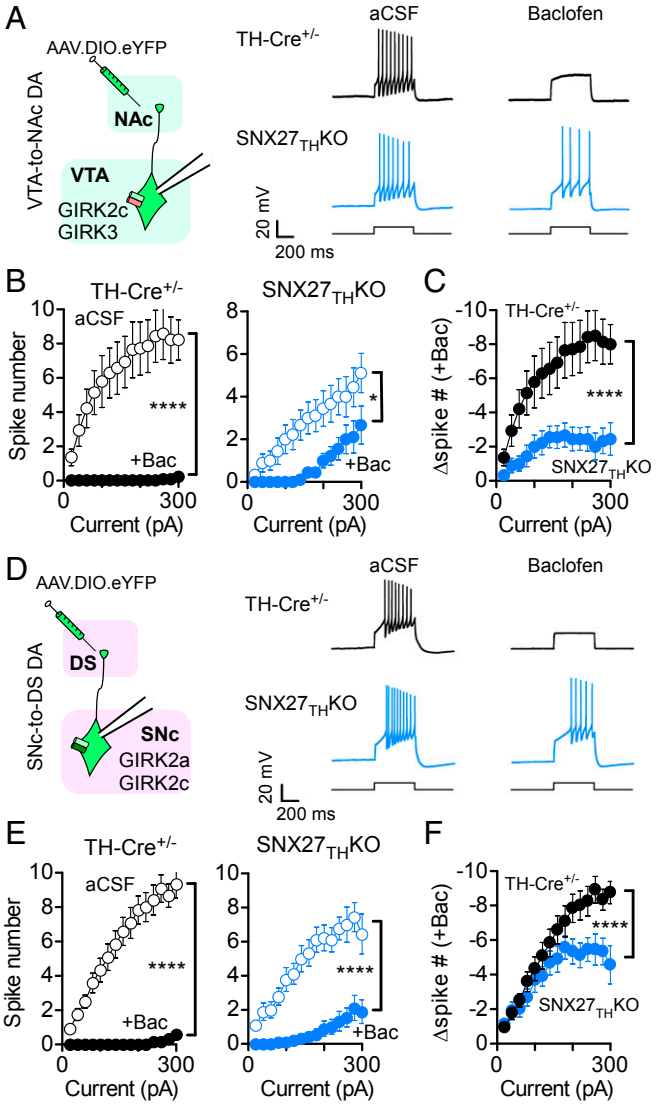

Fig. 2. Attenuation of baclofen-dependent inhibition of firing in VTA-to-NAc DA neurons and SNc-to-DS DA neurons of $SNX27_{TH}$ KO mice. (*A*) Cartoon shows AAV.DIO.eYFP injection into NAc. Representative voltage traces show induced action potentials (280 pA) in the absence and then presence of baclofen for VTA-to-NAc projecting DA neurons. (*B*) Input–output activity plots for VTA-to-NAc projecting DA neurons for the indicated genotype. For TH-$Cre^{+/-}$ mice (n = 12/6 mice), baclofen silenced evoked firing ($^{****}P < 0.0001$). In contrast, silencing is less effective although still statistically significant in $SNX27_{TH}$ KO mice (n = 9/5 mice) ($^{*}P = 0.0231$). (*C*) The baclofen-induced (+Bac) reduction in firing (Δspike #) for $SNX27_{TH}$ KO mice is significantly reduced compared with TH-$Cre^{+/-}$ ($^{****}P < 0.0001$). (*D*) Cartoon shows AAV.DIO.eYFP injection into DS. Voltage traces show induced action potentials (+280 pA) in the absence and then presence of baclofen for SNc-to-DS projecting DA neurons. (*E*) Input-output activity plots for SNc-to-DS projecting DA neurons for the indicated genotype. For TH-$Cre^{+/-}$ DA neurons (n = 12/4 mice), induced firing is suppressed by baclofen ($^{****}P < 0.0001$). For $SNX27_{TH}$ KO mice, baclofen-dependent silencing is incomplete (n = 9/4 mice), although still statistically significant ($^{****}P < 0.0001$). (*F*) Δspike # is reduced in $SNX27_{TH}$ KO mice ($^{****}P < 0.0001$). Two-way repeated-measures ANOVA with asterisks representing P value for interaction between drug/group and current.

number was significantly smaller, compared with TH-Cre$^{+/-}$ mice (interaction between group and current, $P < 0.0001$) (Fig. 2*C*).

SNc-to-DS projecting DA neurons in SNX27$_{TH}$ KO mice also showed impairments of baclofen-dependent inhibition of firing (+baclofen) (Fig. 2*D*). In SNc DA neurons of control TH-Cre$^{+/-}$ mice ($n = 12$ cells/4 mice), we observed robust firing that was silenced by baclofen (interaction between drug and current $P < 0.0001$) (Fig. 2*E*). In SNX27$_{TH}$ KO mice ($n = 9$ cells/4 mice), the firing was also significantly reduced by baclofen (interaction between drug and current, $P < 0.0001$) (Fig. 2*E*) but the ability of baclofen to suppress induced firing (Δspike number) was significantly impaired in SNX27$_{TH}$ KO mice, compared with TH-Cre$^{+/-}$ controls (interaction between group and current, $P < 0.0001$) (Fig. 2*F*). Taken together, these results demonstrate that deletion of SNX27 in both VTA-to-NAc and SNc-to-DS projecting DA neurons leads to an increase in neuronal excitability that manifests, in part, in a reduction in GABA$_B$R-dependent inhibition.

Collectively, the electrophysiological experiments demonstrate that SNX27 plays an important role in regulating GABA$_B$R-dependent inhibition of firing, with little change in resting neuronal excitability (V_{rest}) (*SI Appendix*, Table S2). These cell type- and projection-specific findings in SNX27$_{TH}$ KO mice suggest that GIRK3 is not required for SNX27-dependent regulation of GIRK channels in midbrain DA neurons in vivo.

SNX27 in Midbrain DA Neurons Regulates Locomotor Sensitization to Cocaine. The reduction in receptor-activated GIRK currents in SNX27$_{TH}$ KO mice provides a unique tool to assess whether this functional change in midbrain DA neurons could alter the behavioral response to psychostimulants. Cocaine-dependent locomotor sensitization provides a behavioral test for context-specific enhancement of the response to drug (38). We hypothesized that mice with reduced GIRK currents in midbrain DA neurons would exhibit an increased sensitivity to drug-induced locomotor sensitization. Following acclimatization to saline injections (3 d), we measured the locomotor activity of mice injected with cocaine for the next 5 d (1×/d, i.p.) (Fig. 3*A*), using a typical dosage of 7.5 mg/kg cocaine that was shown previously to induce locomotor sensitization (39). Locomotor activity in SNX27$_{TH}$ KO mice was significantly greater than that in SNX27$^{fl/fl}$ or TH-Cre$^{+/-}$ controls, with a significant interaction between group and day ($P < 0.0001$) (Fig. 3*B*). Significant effects were also detected in both males and females (*SI Appendix*, Fig. S3). To capture the initial difference in locomotor response and acquisition of sensitization with cocaine, we calculated the average change in locomotor activity over the first 2 d of cocaine injections, and found this 2-d change in locomotor activity was significantly greater in SNX27$_{TH}$ KO mice (1,930 ± 191 beam breaks per day, $n = 13$), compared with SNX27$^{fl/fl}$ (585 ± 185 beam breaks per day, $n = 9$, $P < 0.0001$) or TH-Cre$^{+/-}$ (639 ± 107 beam breaks/day, $n = 10$, $P < 0.0001$) (Fig. 3*C*).

We next investigated the effect of a subthreshold dose of cocaine (3.75 mg/kg) on locomotor sensitization. In control SNX27$^{fl/fl}$ or TH-Cre$^{+/-}$ mice, a low dose of cocaine (3.75 mg/kg) was insufficient to induce locomotor sensitization (Fig. 3 *D* and *E*). In contrast, SNX27$_{TH}$ KO mice exhibited locomotor sensitization to the low dose of cocaine, with a significant interaction effect between group and day ($P < 0.0001$) (Fig. 3*D*). Additionally, the 2-d change in locomotor activity was significantly higher in SNX27$_{TH}$ KO mice (521 ± 69 beam breaks per day, $n = 11$) compared with TH-Cre$^{+/-}$ mice (154 ± 99 beam breaks per day, $n = 11$, $P = 0.0103$) or SNX27$^{fl/fl}$ (57 ± 74 beam breaks per day, $n = 11$, $P = 0.0011$) (Fig. 3*E*). Importantly, after a 1-wk withdrawal period, all groups exhibited enhanced locomotor activity with a single cocaine injection, indicating that a low level of sensitization occurred with 3.75 mg/kg cocaine in all groups (Fig. 3*D*). However, the SNX27$_{TH}$ KO mice continued to show the largest locomotor response (Fig. 3*D*). These findings establish that SNX27 expression in midbrain DA neurons functions as a negative regulator of locomotor sensitization to cocaine.

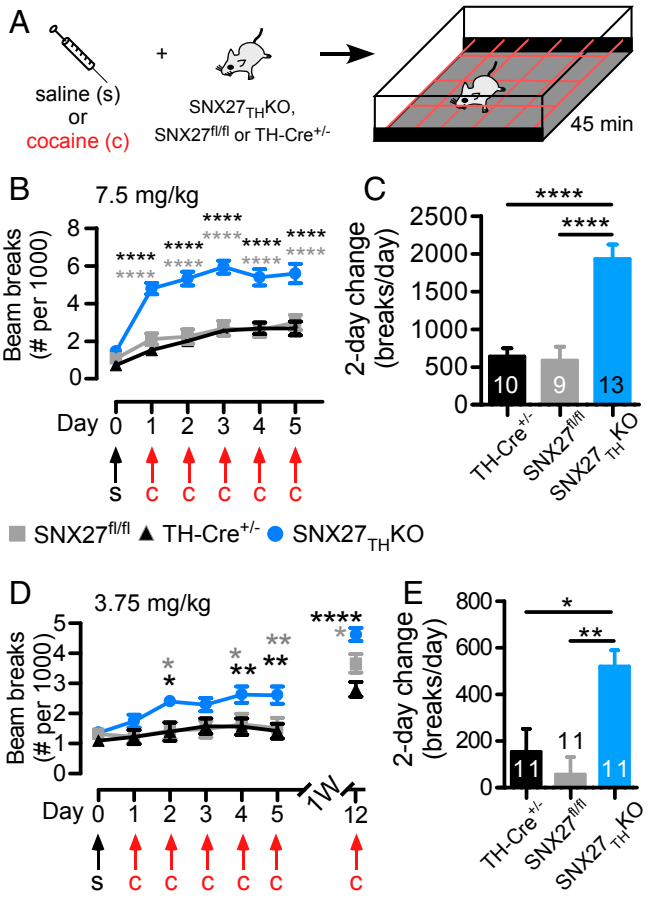

Fig. 3. SNX27$_{TH}$ KO mice exhibit increased sensitivity to locomotor sensitization with cocaine. (*A*) Mice received saline intraperitoneal injections for 3 d, cocaine injections for 5 d, and in some experiments, a single cocaine injection 7 d later. Locomotor activity was measured in an activity chamber after each injection for 45 min. (*B*) Plot shows the number of beam breaks on each day. SNX27$_{TH}$ KO mice ($n = 13$) exhibit increased locomotor response with 7.5 mg/kg cocaine, compared with controls (significant interaction between group and day; days 1–5, gray and black ****$P < 0.0001$) using two-way repeated-measures ANOVA with Bonferroni post hoc test. (*C*) The average change in locomotor activity on day 2 is significantly higher in SNX27$_{TH}$ KO mice ($n = 13$) compared with SNX27$^{fl/fl}$ ($n = 9$, ****$P < 0.0001$) and TH-Cre$^{+/-}$ ($n = 10$, ****$P < 0.0001$). (*D*) SNX27$_{TH}$ KO mice ($n = 11$) exhibit increased locomotor response with 3.75 mg/kg cocaine, compared with SNX27$^{fl/fl}$ ($n = 11$) and TH-Cre$^{+/-}$ ($n = 11$) controls. Same difference in sensitivity exists following 1 wk (1W) withdrawal. (Day 2: gray *$P = 0.0222$, black *$P = 0.0168$; day 4: gray *$P = 0.0186$, black **$P = 0.0096$; day 5: gray **$P = 0.0071$, black **$P = 0.0029$; day 12: gray *$P = 0.0215$, black ****$P < 0.0001$.) (*E*) The average 2-d change in locomotor activity is significantly higher in SNX27$_{TH}$ KO mice compared with TH-Cre$^{+/-}$ (*$P = 0.0103$) or SNX27$^{fl/fl}$ (**$P = 0.0011$) mice.

Projection-Specific Rescue of GABA$_B$R- and D$_2$R-GIRK Currents in SNX27$_{TH}$ KO Mice. In addition to GIRK2c/GIRK3 channels, SNX27 regulates trafficking of other signaling proteins—for example, glutamate receptors and β-adrenergic receptors (40)—raising the possibility that some of the behavioral changes observed in SNX27$_{TH}$ KO may not be due to changes in regulation of GIRK channels. We therefore attempted a functional rescue experiment to determine if the effects of SNX27 are mediated via its interaction with GIRK channels. To accomplish this, we conditionally expressed the GIRK2a subunit, which lacks a PDZ

binding motif but is otherwise identical to GIRK2c (28, 32), in DA neurons lacking SNX27.

We first examined whether expression of GIRK2a was sufficient to restore GIRK currents. Following stereotaxic injection of AAV.DIO.GIRK2a-eYFP into the NAc of $SNX27_{TH}$ KO mice (i.e., "Resc": KO + GIRK2a-YFP), we measured the GIRK currents in DA neurons (Fig. 4 *A–E*). Whereas VTA-to-NAc projecting DA neurons in $SNX27_{TH}$ KO mice (+AAV.DIO.eYFP) have reduced $I_{Baclofen}$ (59.9 ± 15.2 pA, n = 14 cells/6 mice; P = 0.0358) and $I_{Quinpirole}$ (12.0 ± 3.7 pA, n = 11 cells/5 mice, P = 0.0011), the expression of GIRK2a-eYFP in $SNX27_{TH}$ KO mice resulted in large $I_{Baclofen}$ (468 ± 146 pA, n = 7 cells/4 mice, P = 0.0018) and $I_{Quinpirole}$ (109 ± 25 pA, n = 7 cells/4 mice, P = 0.0016) (Fig. 4 *B–D*). The baclofen-dependent hyperpolarization was also restored to control levels by expressing GIRK2a-eYFP in $SNX27_{TH}$ KO mice (Resc) (Fig. 4*E*).

Similar to VTA-to-NAc projecting DA neurons, we asked whether expression of GIRK2a-eYFP could restore GIRK currents in SNc-to-DS DA neurons. In $SNX27_{TH}$ KO mice injected with AAV.DIO.GIRK2a-eYFP into the DS, $GABA_BR$-GIRK ($I_{Baclofen}$ = 656 ± 96 pA, n = 8 cells/5 mice, P < 0.0001) and D_2R-GIRK ($I_{Quinpirole}$ = 119 ± 35 pA, n = 6 cells/5 mice, P = 0.0156) currents were all increased relative to $SNX27_{TH}$ KO receiving control AAV.DIO.eYFP ($I_{Baclofen}$ = 120 ± 23 pA, n = 16 cells/5 mice; $I_{Quinpirole}$ = 21.5 ± 6.8 pA, n = 9 cells/5 mice) (Fig. 4 *F–I*). In the SNc-to-DS DA neurons, $I_{Baclofen}$ exceeded that in control mice (TH-$Cre^{+/-}$ + AAV.DIO.eYFP; P < 0.0001) (Fig. 4 *H* and *I*). Interestingly, $I_{Quinpirole}$ was not significantly smaller in this cohort of $SNX27_{TH}$ KO, compared with control mice (Fig. 4*I*). Expression of GIRK2a in $SNX27_{TH}$ KO DA neurons also restored baclofen-dependent hyperpolarization (Fig. 4*J*).

Finally, expression of GIRK2a-eYFP in $SNX27_{TH}$ KO DA neurons restored $GABA_BR$-dependent inhibition of firing in both

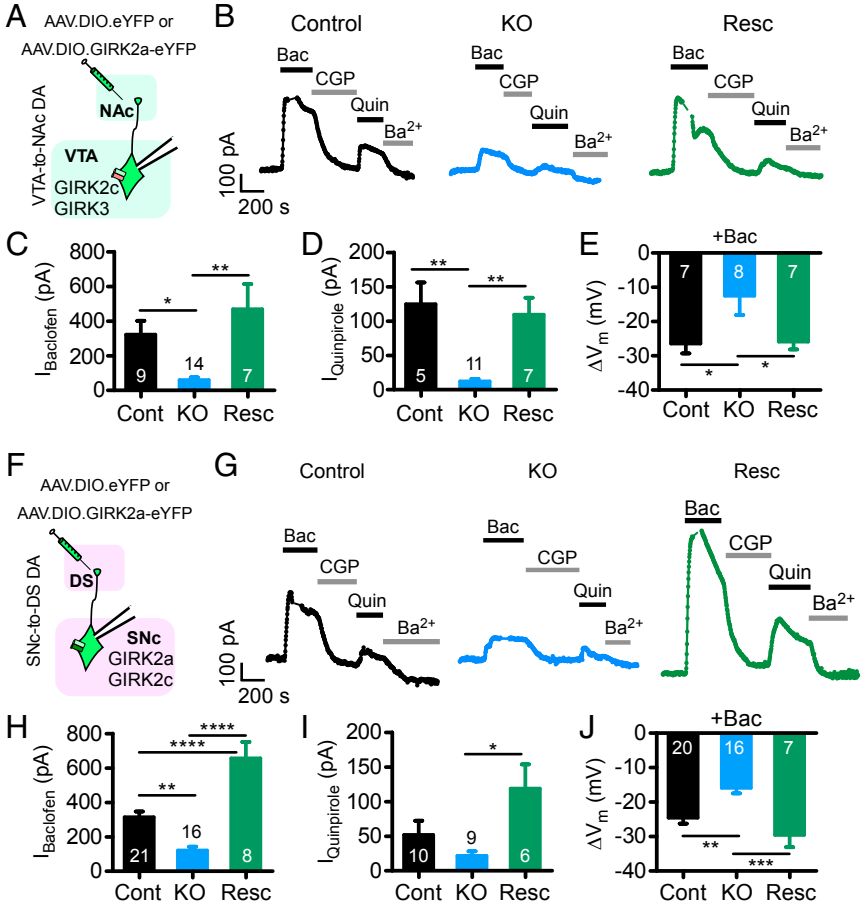

Fig. 4. $GABA_BR$-GIRK and D_2R-GIRK currents are restored by expression of GIRK2a-eYFP in VTA-to-NAc and SNc-to-DS DA neurons of $SNX27_{TH}$ KO mice. (*A*) Cartoon shows virus injection into the NAc. (*B*) Current traces from labeled VTA DA neurons in TH-$Cre^{+/-}$+eYFP (control, black), $SNX27_{TH}$KO+eYFP (KO, blue), and $SNX27_{TH}$KO+GIRK2a-eYFP (Resc, green) mice show response to bath application of (±)-baclofen (300 μM), CGP54626 (5 μM), (-)-quinpirole (100 μM), or Ba^{2+} (1 mM). (*C*) $I_{Baclofen}$ is significantly smaller in VTA-to-NAc projecting DA neurons of KO mice (n = 14/6 mice; *P = 0.0358) compared with control mice (n = 9/5 mice). $I_{Baclofen}$ is restored in KO mice expressing GIRK2a-eYFP (Resc, n = 7/4 mice, **P = 0.0018). (*D*) $I_{Quinpirole}$ in VTA-to-NAc projecting DA neurons is decreased in KO mice (n = 11/5 mice, **P = 0.0011), compared with control mice (n = 5/4 mice), and is restored in KO mice expressing GIRK2a-eYFP (Resc, n = 7/4 mice, **P = 0.0016). (*E*) ΔV_m (+Bac) is reduced in KO mice (n = 8/4 mice, *P = 0.0497) compared with control mice (n = 7/4 mice), but is restored in KO mice expressing GIRK2a-eYFP (Resc, n = 7/4 mice, *P = 0.0497). (*F*) Cartoon shows virus injection into DS. (*G*) Current traces from labeled SNc DA neurons in TH-$Cre^{+/-}$+eYFP (control, black), $SNX27_{TH}$KO+eYFP (KO, blue), and KO+GIRK2a-eYFP (Resc, green) mice. (*H*) $I_{Baclofen}$ is decreased in SNc DA neurons of KO mice (n = 16/5 mice, **P = 0.0026) compared with control mice (n = 21/4 mice), and is restored in KO mice expressing GIRK2a-eYFP (n = 8/5 mice, ****P < 0.0001). (*I*) $I_{Quinpirole}$ in KO mice (n = 9/5 mice, P > 0.05) is similar to control mice (n = 10/4 mice), but is significantly increased in KO mice expressing GIRK2a-eYFP (Resc, n = 6/5 mice, *P = 0.0156). (*J*) ΔV_m (+Bac) is reduced in KO mice (n = 16/5 mice, **P = 0.0013) compared with control mice (n = 20/5 mice), and is restored in KO mice expressing GIRK2a-eYFP (n = 7 cells/4 mice, ***P = 0.0005). One-way ANOVA with Bonferroni post hoc test (*C*, *D*, *H*, and *I*) or one-way ANOVA with Holm–Sidak post hoc test (*E* and *J*).

VTA-to-NAc (Fig. 5 *A–D*) and SNc-to-DS projecting DA (Fig. 5 *E–H*) neurons. In VTA-to-NAc DA neurons, this effect of baclofen was markedly attenuated in $SNX27_{TH}$ KO mice but restored to wild-type levels in the GIRK2a Resc mice (n = 7 cells/4 mice; interaction between drug and current, $P < 0.0001$) (Fig. 5 *A* and *C*). In SNc-to-DS DA neurons, GIRK2a Resc similarly restored the effect of baclofen (n = 7 cells/4 mice; interaction between drug and current $P < 0.0001$) (Fig. 5 *E* and *G*). Interestingly, the Δspike number with baclofen for the $SNX27_{TH}$ KO was not much smaller than control or Resc mice (Fig. 5*H*), perhaps due to larger $I_{Baclofen}$ in SNc DA neurons (Fig. 4*H*).

Thus, three different measures of GIRK function indicated that expression of GIRK2a-eYFP in DA neurons lacking SNX27 can restore GIRK signaling. Although SNX27 interacts with a diverse set of proteins, its effects on evoked firing in the presence of baclofen can be linked directly to GIRK channels.

SNX27 Acts via GIRK Channels in VTA DA Neurons to Regulate Locomotor Sensitization to Cocaine. The mesolimbic DA pathway has long been implicated in addiction (2). We therefore interrogated the role of VTA-to-NAc DA neurons in the locomotor response to cocaine. To address this, we first attempted to study the effect of a pathway-specific rescue on cocaine-dependent locomotor

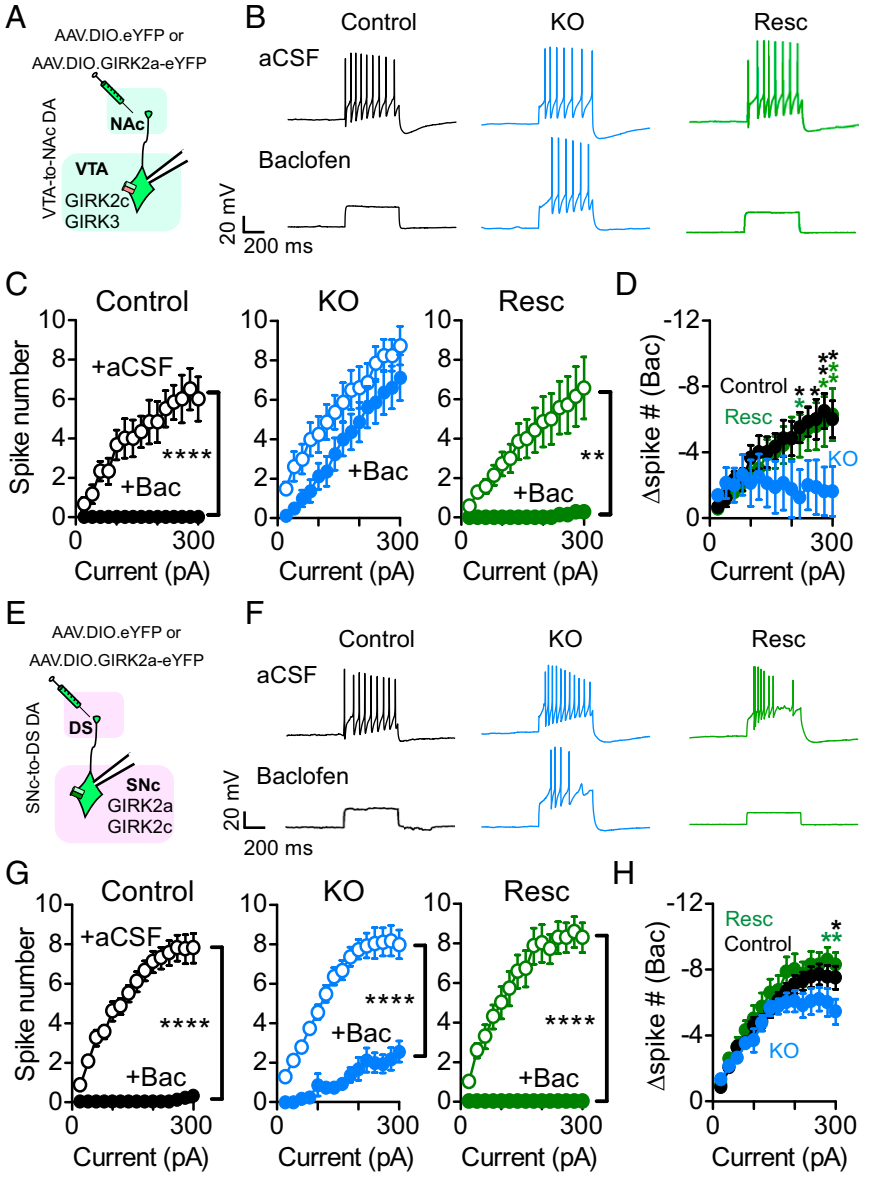

Fig. 5. $GABA_BR$-dependent inhibition of firing is restored in $SNX27_{TH}$ KO mice expressing GIRK2a-eYFP in both VTA-to-NAc and SNc-to-DS DA projection neurons. (*A*) Cartoon shows virus injection into the NAc. (*B*) Voltage traces show induced spikes (+300 pA) in the absence and then presence of baclofen (300 μM) for TH-$Cre^{+/-}$+eYFP (control, black), $SNX27_{TH}$KO+eYFP (KO, blue), and $SNX27_{TH}$KO+GIRK2a-eYFP (Resc, green) mice. (*C*) Baclofen strongly suppresses firing in VTA-to-NAc DA neurons from control mice (n = 6/5 mice; $^{****}P < 0.0001$) and KO mice expressing GIRK2a-eYFP (Resc) (n = 7/4 mice; $^{**}P = 0.0016$) but not in KO (n = 8/5 mice; $P = 0.1408$). (*D*) Δspike # is significantly smaller in KO mice, compared with control mice and KO mice expressing GIRK2a-eYFP (Resc). Bonferroni post hoc test at indicated current ($^{*}P < 0.05$, $^{**}P < 0.01$). (*E*) Virus injection into the DS. (*F*) Voltage traces show induced spikes (+300 pA) in the absence and presence of baclofen (300 μM) for SNc-to-DS DA neurons. (*G*) Baclofen strongly suppresses firing in SNc-to-DS DA neurons in control mice (n = 20/5 mice; $^{****}P < 0.0001$) and Resc mice (n = 7/4 mice; $^{****}P < 0.0001$), but to a lesser extent in $SNX27_{TH}$ KO mice (n = 16/5 mice; $^{****}P < 0.0001$). (*H*) Δspike # is significantly smaller in KO mice compared with control mice and Resc mice. Bonferroni post hoc test at indicated current ($^{*}P < 0.05$).

sensitization. $SNX27_{TH}$ KO mice received AAV.DIO.eYFP or AAV.DIO.GIRK2a-eYFP injections into the NAc and were then examined for locomotor sensitization with a low concentration of cocaine, 3.75 mg/kg (Fig. 6*A*, cohort 1). Unexpectedly, locomotor sensitization in the $SNX27_{TH}$ KO mice injected with GIRK2a-eYFP into the NAc was indistinguishable from that of $SNX27_{TH}$ KO alone (*SI Appendix*, Fig. S4). However, a post hoc analysis of the number of retrogradely labeled DA neurons in the VTA indicated a low percentage of YFP-expressing DA neurons, suggesting an insufficient number of VTA DA neurons expressed GIRK2a-eYFP (Fig. 6*A*). To explore this possibility, we plotted the 2-d change in locomotor activity as a function of the mean number of YFP^+ cells in the VTA for each mouse, and observed an inverse correlation (Fig. 6*B*). That is, mice with a greater number of neurons positive for GIRK2a-YFP tended to respond more like control mice (i.e., rescued) than KO mice.

We therefore used an alternative strategy of injecting AAV.DIO.eYFP or AAV.DIO.GIRK2a-eYFP bilaterally into the VTA of TH-$Cre^{+/-}$ mice or $SNX27_{TH}$ KO mice (Fig. 6*A*, cohort 2). Expression of GIRK2a in the VTA restores $I_{Baclofen}$ in VTA DA neurons of $SNX27_{DA}$ KO mice (31). Importantly, the expression of YFP^+ neurons in the VTA was much more robust (Fig. 6*A*). Following AAV injection (4–5 wk), mice were tested for locomotor sensitization with the subthreshold dose of 3.75 mg/kg cocaine (Fig. 6*C*). As shown previously, $SNX27_{TH}$ KO (+AAV.DIO.eYFP) mice exhibit elevated locomotor sensitization relative to TH-$Cre^{+/-}$ (+AAV.DIO.eYFP) control mice on all days (Fig. 6*C*). This enhanced sensitivity to cocaine was absent in $SNX27_{TH}$ KO mice expressing GIRK2a-eYFP on days 1–5 ($P = 0.1303$ vs. TH-$Cre^{+/-}$) (Fig. 6*C*). Additionally, locomotor sensitization was significantly greater in $SNX27_{TH}$ KO (+AAV.DIO.eYFP) mice than in $SNX27_{TH}$ KO mice expressing GIRK2a-eYFP (+AAV.DIO.GIRK2a-eYFP) on day 12 ($P < 0.0001$) (Fig. 6*C*), demonstrating a persistent effect of exogenous GIRK2a-eYFP.

Similarly, in $SNX27_{TH}$ KO mice expressing GIRK2a-eYFP (Resc), the 2-d change in locomotor activity was smaller (370 ± 63 beam breaks per day, $n = 15$) than $SNX27_{TH}$ KO (+AAV.DIO.eYFP) ($P = 0.0219$) but similar to that in TH-$Cre^{+/-}$ control mice (+AAV.DIO.eYFP) ($P = 0.7744$) (Fig. 6*D*). In $SNX27_{TH}$ KO mice, the 2-d change in locomotor activity (696 ± 113 beam breaks per day, $n = 11$) was significantly higher compared with TH-$Cre^{+/-}$ (+AAV.DIO.eYFP) control mice (254.9 ± 61.97 beam breaks per day, $n = 19$, $P = 0.0008$). These findings demonstrate that, irrespective of the diverse binding targets of SNX27 (40), the behavioral effects of its deletion from midbrain DA neurons on locomotor sensitization to cocaine can be fully reversed by exogenous expression of GIRK2a in primarily VTA DA neurons. Thus, the role of SNX27 in VTA DA neurons in changing the sensitivity to locomotor sensitization with cocaine is mediated primarily by SNX27-dependent regulation of GIRK channels.

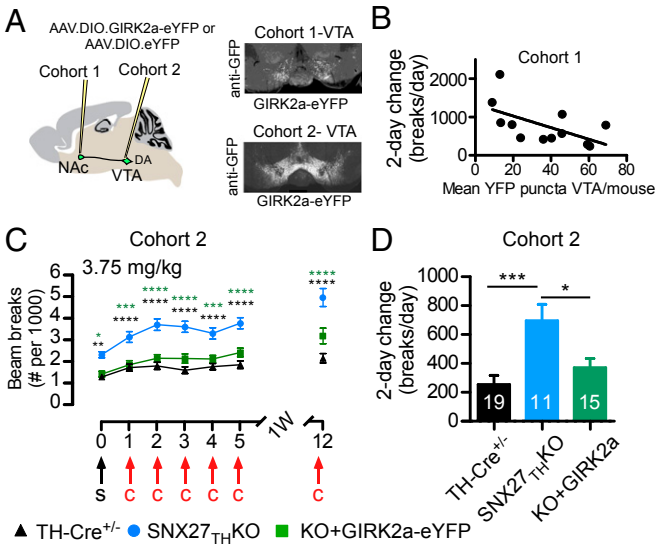

Fig. 6. GIRK2a-YFP expressed in VTA DA neurons of $SNX27_{TH}$ KO mice reduces locomotor sensitization to cocaine. (*A*) Schematic shows in vivo virus injection into NAc (cohort 1) or the VTA (cohort 2). Images show representative examples of GIRK2a-YFP fluorescence in midbrain of cohort s1 and 2. (*B*) Mean number of YFP^+ puncta in VTA is plotted as a function of the 2-d change in locomotor activity for each mouse injected with AAV.DIO.GIRK2a-eYFP into the NAc (*SI Appendix*, Fig. S1). Line shows linear fit ($r^2 = 0.3365$, $P = 0.048$, Pearson correlation). (*C*) Plot of the average number of beam breaks per day for the indicated genotype using 3.75 mg/kg cocaine. Locomotor sensitization is enhanced in KO+eYFP mice ($n = 11$, blue) compared with TH-$Cre^{+/-}$+eYFP (control, $n = 19$, black), but not in KO mice expressing GIRK2a-eYFP (Resc, $n = 15$, green) (*$P < 0.05$, **$P < 0.01$, ***$P < 0.001$, ****$P < 0.0001$ using two-way repeated-measures ANOVA with Bonferroni post hoc test). (*D*) The 2-d change in locomotor activity is significantly higher in KO mice, compared with control mice ($n = 19$, ***$P = 0.0008$) as well as Resc mice (KO+GIRK2a-eYFP, $n = 15$, *$P = 0.0219$). Resc mice are not significantly different from control mice ($P = 0.7744$).

Discussion

Changes in the excitability of midbrain DA neurons are a central component of the subcellular alterations that underlie addiction to abused drugs, as well as of other neurological diseases, such as Parkinson disease and epilepsy. In the present study, we used cell-type and projection-specific labeling techniques to elucidate a role for SNX27, through its regulation of GIRK channels in primarily VTA DA neurons, in determining the sensitivity of mice to cocaine-dependent locomotor sensitization. Targeting a specific pathway and population of DA neurons provides more granularity in the circuit involved in addiction, further clarifying the role of a diverse set of midbrain neurons.

SNX27 Regulation of GIRK2c and GIRK3 Channels in the Brain. SNX27 contains three functional domains: a PDZ domain, a PX domain, and a FERM-like domain (30, 41). The PX domain selectively binds phosphatidylinositol-3-phosphate (PI3P), which is enriched in early endosomes (EE), and therefore targets SNX27 to the EE with GIRK channels and other proteins (28, 42). The PDZ domain mediates the association of SNX27 with the PDZ-binding motif of other proteins. The PDZ domain of SNX27 also binds to and regulates other membrane signaling proteins, including glutamate receptors and several different G protein-coupled receptors (GPCRs) (42–49). In an elegant set of biochemical studies, Temkin et al. (45) showed that SNX27 functions as an adapter between the retromer complex, which includes VPS29, VPS35, VPS26, and the WASH complex, and PDZ ligand-containing cargoes. RNAi knockdown of SNX27 in HEK293 cells reduced recycling of β2AR to the plasma membrane following agonist stimulation (45). In neurons, SNX27 may also be involved in forward trafficking of cargo proteins to the plasma membrane. Hussain et al. (47) found that loss of SNX27 in hippocampal neurons impairs recruitment of surface AMPARs during chemical LTP. Similarly, Wang et al. (50) demonstrated that *Snx27*$^{+/-}$ mice also exhibit a reduction in expression of glutamate receptors (NMDAR and AMPAR) coincident with defects in synaptic function. Thus, SNX27 promotes PDZ-directed plasma membrane sorting through the retromer tubule via its association with the WASH complex and certain PDZ-ligand–containing proteins (45).

The PDZ domain in SNX27 is highly specific for certain class I PDZ ligands, which are found in both GIRK2c and GIRK3 subunits (28, 51). The role of SNX27 in regulating forward trafficking of GIRK channels in SNc DA neurons that lack GIRK3 was

unknown (32). We discovered that $GABA_BR$- and D_2R-activated GIRK currents are significantly smaller in both SNc and VTA DA neurons of $SNX27_{TH}$ KO mice. These findings suggest SNX27 may control forward trafficking of both GIRK2c-containing and GIRK3-containing channels because VTA DA neurons express GIRK2c and GIRK3, while SNc DA neurons express GIRK2a and GIRK2c subunits (15, 28, 32, 51). On the other hand, coexpression of SNX27 with GIRK channels in HEK293 cells (28) or in cultured hippocampal neurons (51) reduces receptor-activated GIRK currents, suggesting that overexpression of SNX27 exerts a negative regulatory effect on GIRK3-containing channels, perhaps due to the lysosomal targeting motif in GIRK3 (52). In addition to SNX27, the GIRK3 subunit also contributes to the behavioral response to drugs. Mice lacking GIRK3 in the VTA show reduced response to ethanol and increased drinking (53) and reduced morphine-induced motor activity (54), although these studies did not distinguish GIRK3 expression in VTA GABA or DA neurons. Ablation of GIRK3 in VTA DA neurons prevents activity-dependent potentiation of $GABA_BR$-GIRK currents (55). Taken together, these findings indicate that SNX27 is directly involved in recycling GIRK channels from early endosomes to the plasma membrane in DA neurons. Future studies will need to address whether up-regulation of SNX27 in VTA DA neurons also leads to reduced GIRK currents.

Role of SNX27 in DA Neurons for Cocaine Sensitization. Our experiments demonstrate that deletion of SNX27 selectively from DA neurons ($SNX27_{TH}$ KO) markedly enhances locomotor sensitization to cocaine; that is, $SNX27_{TH}$ KO mice are susceptible to the addictive effects of a low dose of cocaine. Ablation of SNX27 in only TH-expressing neurons results in significantly smaller receptor-activated GIRK currents in I_h^+ SNc DA and VTA DA neurons. Midbrain DA neurons (9, 56) can be subdivided into phenotypically distinct I_h^+ and I_h^- DA neurons that project to specific brain regions (10–12). Generally, I_h^+ SNc and VTA DA neurons project to the DS and NAc lateral shell, respectively (10–12). Thus, an increase in excitability of both neurons could contribute to the enhanced sensitivity to cocaine. Although the reduction of the GIRK current in the VTA-to-NAc pathway of KO mice could be functionally rescued by expression of GIRK2a in the NAc, it was not sufficient to rescue (i.e., reduce) cocaine sensitivity to control levels. While targeted expression of GIRK2a in VTA DA neurons of KO mice does restore $GABA_BR$-GIRK currents (31), as well as decreases cocaine sensitivity (present study), one caveat is worth noting. Injection of AAV DIO-GIRK2a-eYFP into the VTA of KO mouse will lead to expression of GIRK2a in all VTA DA neurons, including those that project to cortex (i.e., meso-cortical) and those that project to other limbic structures (i.e., amygdala) (10). These VTA DA projection neurons vary significantly in their physiology; for example, mesoprefrontal DA neurons express very low levels of GIRK2 and D_2R (11). Thus, viral expression of GIRK2a in these neurons likely leads to GIRK expression that exceeds physiological levels. However, our experimental tools were not sufficient to isolate the behavioral effects of this change. Developing viral vectors that can retrograde efficiently and lead to expression of high quantities (i.e., sufficient to alter behavior) of GIRK channels should allow their role in these distinct VTA DA neuron pathways to be disambiguated.

In support of our findings implicating VTA DA neurons, intra-VTA injection of stimulants is sufficient to produce sensitization (57, 58). Furthermore, designer receptors exclusively activated by designer drug (DREADD)-dependent activation of VTA DA neurons projecting to the NAc induce hyperactivity, whereas stimulation of the SNc-to-DS projecting neurons produces little effect on locomotion (59), consistent with intra-NAc injections of amphetamine eliciting locomotor activity (60). However, recent studies using optogenetic and chemogenetic techniques suggest a more complex role of these two pathways. For example, a recent study with DREADD-dependent activation in a five-choice serial reaction time task did not elicit impulsivity (61), although prior studies suggested VTA-to-NAc DA neurons are involved in impulsivity (62–64). In addition, mice learn to self-administer optogenetic stimulation of both VTA and SNc neurons (7, 14), implying that SNc DA neurons can function like VTA DA neurons in reward and addiction (13, 14). Our results provide evidence to implicate the activity of VTA DA neurons in determining the sensitivity of the locomotor response to cocaine.

In our electrophysiology experiments, we found that AAV.DIO.GIRK2a-eYFP virus injected into $SNX27_{TH}$ KO mice led to substantially larger GIRK currents than in TH-Cre mice receiving control virus. Thus, our "rescue" experiments are in some cases more like overexpression. Because $SNX27_{TH}$ KO mice displayed small GIRK currents and enhanced locomotor sensitization to cocaine, one might predict that overexpression of GIRK2a-eYFP would result in reduced (i.e., protective) locomotor sensitization. However, rescued $SNX27_{TH}$ KO mice responded to cocaine behaviorally similar to control mice. Similarly, the baclofen-dependent hyperpolarization in rescued neurons was similar to control. Future experiments can address the impact of increased GIRK expression by conducting a dose–response to cocaine in TH-Cre mice that have received intra-VTA injections of AAV.DIO.GIRK2a-eYFP.

The present findings establish SNX27 acting via GIRK channels as a new player in the pathophysiology of addiction. Our findings add to increasing evidence that $GABA_BR$-GIRK currents play a critical role in the development of addictive behavior to cocaine (16). For example, exposure to psychostimulants has been shown to induce alterations in $GABA_BR$-GIRK currents (22–25, 65). In another study, D_1R-expressing medium spiny neurons in the NAc project to the VTA and form primarily $GABA_BR$-dependent synapses on VTA DA neurons (66). Deletion of $GABA_BRs$ from VTA DA neurons enhances the locomotor sensitization to cocaine (66). Additionally, mice lacking the GIRK2 subunit in DA neurons exhibit a similarly enhanced locomotor response to cocaine (26). Thus, deletion of the $GABA_BR$ or its effector (i.e., GIRK2) in DA neurons achieves a similar phenotype as deletion of SNX27. SNX27 provides a possible drug-dependent pathway for regulating $GABA_BR$-GIRK currents, situated as an upstream regulator of GIRK channels. Interestingly, exposure to psychostimulants up-regulates the mRNA for the SNX27b splice variant in the cortex, raising the possibility of focusing on SNX27 as a therapeutic target for treating addiction (30).

While we have focused on $GABA_B$ receptors, dopamine D_2 receptors also couple to GIRK channels in VTA DA neurons (21, 67) and are expressed in the presynaptic and somatodendritic compartments of VTA DA neurons, with the notable exception of mesoprefrontal DA neurons (11, 68). D_2 autoreceptors regulate the locomotor sensitization response to cocaine (69) and their function in VTA DA neurons is altered by psychostimulant exposure (70), highlighting the importance of understanding how D_2 receptors are regulated in these neurons. It is an open question whether GIRK channels activated by different GPCRs, such as $GABA_BR$ or D_2R, belong to a common pool or are separate populations that are regulated independently. Our electrophysiology experiments indicate that SNX27 regulates GIRK channels coupled with D_2Rs as well as with $GABA_BRs$. In both cases, the absence of SNX27 decreased agonist-evoked GIRK currents, suggesting these GIRK channels are regulated by SNX27 as a single population.

Our results highlight an important role for SNX27-dependent regulation of GIRK channels in the context of addiction. SNX27 has been also implicated in other human disorders, including Alzheimer's disease, epilepsy, and Down's syndrome. Exome analysis revealed homozygous mutations in SNX27 in patients who presented symptoms of intractable myoclonic epilepsy and lack of psychomotor development (71). In Down's syndrome brains, there is

reduced expression of SNX27 and a putative transcription factor for SNX27, CCAAT/enhancer binding protein β (C/EBPβ) (50). Up-regulating SNX27 in the hippocampus of Down's syndrome mice rescues synaptic and cognitive deficits (50). Thus, elucidating the function of SNX27 in the brain can provide new strategies for developing treatments for a variety of neurological diseases.

Materials and Methods

Generation of Conditional SNX27 KO Mice. $SNX27_{DA}$ KO mice were derived from breeding *Snx27*$^{fl/fl}$ and DAT-Cre$^{+/-}$ mice, as previously described (31). As the selection of Cre-driver lines for targeting midbrain DA neurons has been debated (34, 35), we created a second line of SNX27 KO mice using Bac-transgenic TH-Cre$^{+/-}$ line ($SNX27_{TH}$ KO) (36, 37). Bac-transgenic mice expressing Cre under control of the *Th* promoter (TH-Cre), backcrossed ≥5 generations into C57BL/6 (36, 37), were a gift from Ming-Hu Han, Icahn School of Medicine at Mount Sinai, New York. Female *Snx27*$^{fl/fl}$ mice were crossed with male TH-Cre$^{+/-}$ mice to generate *Snx27*$^{fl/+}$:TH-Cre$^{+/-}$ mice. Male *Snx27*$^{fl/+}$:TH-Cre$^{+/-}$ mice were crossed with female *Snx27*$^{fl/fl}$ mice to generate *Snx27*$^{fl/fl}$:TH-Cre$^{+/-}$ ($SNX27_{TH}$ KO) mice. $SNX27_{TH}$ KO male mice were bred with *Snx27*$^{fl/fl}$ female mice to produce $SNX27_{TH}$ KO experimental mice and *Snx27*$^{fl/fl}$ littermate controls. TH-Cre$^{+/-}$ male mice were bred separately with C57BL/6 female mice to generate TH-Cre$^{+/-}$ control mice for experiments. Tail biopsies were collected at weaning and genotyped by a commercial vendor (Transnetyx).

All aspects of animal care and experimentation were approved by the Institutional Animal Care and Use Committee at the Icahn School of Medicine at Mount Sinai, New York. Animals were housed in a temperature- and humidity-controlled nonbarrier facility with ad libitum access to water and standard chow, on a standard (light 0700–1900 hours) light–dark cycle.

Stereotaxic Surgery. Mice were anesthetized via intraperitoneal injection of ketamine (100 mg/kg) and xylazine (10 mg/kg), confirmed by absence of pedal pain reflex, and placed in a stereotaxic frame. A midline incision was made to expose the skull and burr holes overlying the injection sites were made with a dental drill. A 33-gauge needle was used to infuse 0.5 μL of AAV5.EF1a.DIO.eYFP or AAV2/5.EF1a.DIO.Girk2a-eYFP virus per side at 0.1 μL/min, followed by a 2- to 5-min wait before slowly retracting the needle. VTA coordinates (relative to bregma) are as follows: 0° angle, M-L ± 0.5 mm, A-P −3.0 mm, D-V −4.5 mm. NAc coordinates (relative to bregma) are as follows: ± 10° angle, M-L ± 2.0 mm, A-P +1.6 mm, D-V −4.4 mm. DS coordinates (relative to bregma) are as follows: 0° angle, M-L ±1.9 mm, A-P +1.0 mm, D-V −2.2 mm. Scalp wounds were sutured and animals were allowed to recover ≥20 d in their home cage before electrophysiology or behavior experiments.

Before electrophysiological labeling and rescue experiments using AAV.DIO.eYFP or AAV.DIO.GIRK2a-eYFP viruses injected into the NAc or DS, we validated the injection coordinates using anti-GFP antibody (ThermoFisher #A6455). NAc coordinates are centered at the NAc lateral shell, but staining typically included the NAc core and medial shell. DS coordinates are centered at the dorsal portion of the DS, with no contamination of the ventral striatum.

Viral Vectors. Girk2a-eYFP, in which GIRK2a is fused to eYFP, was subcloned into pAAV-EF1a.DIO.eYFP.WPRE.hGH.pA (Addgene plasmid 20296) and made into high titer (≥1×10^{12} copies per milliliter) AAV2/5 by the Salk Institute Vector Core, as previously described (31). Stock high titer (≥1×10^{12} copies per milliliter) AAV5.EF1a.DIO.eYFP.WPRE.hGH control viruses were obtained from University of Pennsylvania or University of North Carolina at Chapel Hill vector cores.

Electrophysiology. Artificial cerebrospinal fluid (aCSF) contained the following: NaCl 119 mM, D-glucose 11 mM, $NaHCO_3$ 26.2 mM, KCl 2.5 mM, $MgCl_2$ 1.3 mM, NaH_2PO_4 1 mM, $CaCl_2$ 2.5 mM (pH 7.3). Sucrose aCSF was prepared containing the following: sucrose 207 mM, D-glucose 11 mM, $NaHCO_3$ 26.2 mM, KCl 2.5 mM, $MgCl_2$ 1.3 mM, NaH_2PO_4 1 mM, $CaCl_2$ 2.5 mM (pH 7.3), aerated with 95% O_2/5% CO_2. Coronal slices (250 μm) of midbrain were prepared from male and female mice aged 6–12 wk in aerated ice-cold sucrose-aCSF (*SI Appendix, Supplemental Materials and Methods*). Briefly, DA neurons in the VTA or SNc were identified by eYFP/GFP fluorescence using a Zeiss Axioskop epifluorescent microscope, and recorded via whole-cell patch clamp. Electrophysiology data were quantified in Python 3 (Python Software Foundation) using the numpy, matplotlib, and stfio (72) modules, and plotted using Prism (GraphPad Software).

Behavioral Measurements. For locomotor sensitization studies, age-matched cohorts of male and female mice were transferred to a nonbarrier vivarium near the testing apparatus ≥2 wk before testing. On each day of the experiment, mice were brought into the testing room ≥1 h before testing. Experiments were performed during the light cycle (0700–1900 hours) at a consistent time of day. For 3 d, mice received an intraperitoneal injection of 10 μL sterile PBS per gram body weight and immediately tested for locomotor activity in a "PAS-Home Cage" (San Diego Instruments). On 5 subsequent testing days (plus additional challenge days), mice received an intraperitoneal injection of 3.75 mg/kg or 7.5 mg/kg cocaine in the same volume of PBS and total beam breaks over 45 min per day were measured. The change in locomotor activity during the first 2 d was calculated by measuring the slope between day 2 and day 0 [(day 2 – day 0)/2)].

Immunohistochemistry and Protein Biochemistry. Mice were deeply anesthetized via isoflurane inhalation and transcardially perfused with PBS, followed by 4% paraformaldehyde in PBS. The brain was removed and fixed overnight in 4% paraformaldehyde in PBS, then transferred to PBS. Next, 60-μm coronal sections of the appropriate brain region were made using a vibratome and stained using rabbit anti-GFP (ThermoFisher #A6455) followed by donkey anti-rabbit IgG (Jackson ImmunoResearch #711-545-152) Sections were mounted on glass slides and imaged using a Zeiss epifluorescent microscope and analyzed with NIH ImageJ. Midbrain punches were prepared for Western analysis, as described in *SI Appendix, Supplemental Materials and Methods*.

Statistical Analyses. Data analyses were performed in Prism 7.0 (GraphPad Software). Average data are reported as mean ± SEM. For voltage-clamp data, nonparametric tests were used: the Mann–Whitney test for two groups, and the Kruskal–Wallis test with Dunn post hoc tests for three groups. For current-clamp data, one-way ANOVA or two-way repeated-measures ANOVA with Bonferroni post hoc tests were used. For locomotor sensitization, two-way repeated-measures ANOVA with Bonferroni post hoc tests was used. The 2-d change in locomotor activity was analyzed by one-way ANOVA with Bonferroni post hoc tests. *$P < 0.05$, **$P < 0.01$, ***$P < 0.001$, and ****$P < 0.0001$ were considered significant for all analyses. Actual P values are reported, if available. For complete statistical results, see *SI Appendix, Supplemental Materials and Methods*.

ACKNOWLEDGMENTS. We thank members of the P.A.S. laboratory for reading the manuscript; and Profs. Scott Russo, Ming-Hu Han, and Yasmin Hurd for advice. This work was supported by National Institute on Drug Abuse Grant R01-DA037170 (to P.A.S. and S.J.M.); National Institute on Drug Abuse Grant AA018734 (to P.A.S.); National Institute of General Medical Sciences Training Grant T32GM062754 (to R.A.R.); Brain & Behavior Research Foundation's 2017 NARSAD Young Investigator Grant (to X.L.); and a predoctoral National Research Service Award Fellowship F30-DA039637 from National Institute on Drug Abuse (to R.A.R.).

1. Lüscher C, Malenka RC (2011) Drug-evoked synaptic plasticity in addiction: From molecular changes to circuit remodeling. *Neuron* 69:650–663.
2. Di Chiara G, Imperato A (1988) Drugs abused by humans preferentially increase synaptic dopamine concentrations in the mesolimbic system of freely moving rats. *Proc Natl Acad Sci USA* 85:5274–5278.
3. Moghaddam B, Bunney BS (1989) Differential effect of cocaine on extracellular dopamine levels in rat medial prefrontal cortex and nucleus accumbens: Comparison to amphetamine. *Synapse* 4:156–161.
4. Bradberry CW, Roth RH (1989) Cocaine increases extracellular dopamine in rat nucleus accumbens and ventral tegmental area as shown by in vivo microdialysis. *Neurosci Lett* 103:97–102.
5. Nestler EJ (2005) Is there a common molecular pathway for addiction? *Nat Neurosci* 8:1445–1449.
6. Lüscher C, Ungless MA (2006) The mechanistic classification of addictive drugs. *PLoS Medicine* 3:e437.
7. Tsai HC, et al. (2009) Phasic firing in dopaminergic neurons is sufficient for behavioral conditioning. *Science* 324:1080–1084.
8. Witten IB, et al. (2011) Recombinase-driver rat lines: Tools, techniques, and optogenetic application to dopamine-mediated reinforcement. *Neuron* 72:721–733.
9. Johnson SW, North RA (1992) Two types of neurone in the rat ventral tegmental area and their synaptic inputs. *J Physiol* 450:455–468.
10. Lammel S, Lim BK, Malenka RC (2014) Reward and aversion in a heterogeneous midbrain dopamine system. *Neuropharmacology* 76:351–359.
11. Lammel S, et al. (2008) Unique properties of mesoprefrontal neurons within a dual mesocorticolimbic dopamine system. *Neuron* 57:760–773.
12. Lammel S, Ion DI, Roeper J, Malenka RC (2011) Projection-specific modulation of dopamine neuron synapses by aversive and rewarding stimuli. *Neuron* 70:855–862.
13. Rossi MA, Sukharnikova T, Hayrapetyan VY, Yang L, Yin HH (2013) Operant self-stimulation of dopamine neurons in the substantia nigra. *PLoS One* 8:e65799.

14. Ilango A, et al. (2014) Similar roles of substantia nigra and ventral tegmental dopamine neurons in reward and aversion. *J Neurosci* 34:817–822.
15. Cruz HG, et al. (2004) Bi-directional effects of GABA(B) receptor agonists on the mesolimbic dopamine system. *Nat Neurosci* 7:153–159.
16. Rifkin RA, Moss SJ, Slesinger PA (2017) G protein-gated potassium channels: A link to drug addiction. *Trends Pharmacol Sci* 38:378–392.
17. Reuveny E, et al. (1994) Activation of the cloned muscarinic potassium channel by G protein beta gamma subunits. *Nature* 370:143–146.
18. Logothetis DE, Kurachi Y, Galper J, Neer EJ, Clapham DE (1987) The beta gamma subunits of GTP-binding proteins activate the muscarinic K+ channel in heart. *Nature* 325:321–326.
19. Wickman KD, et al. (1994) Recombinant G-protein beta gamma-subunits activate the muscarinic-gated atrial potassium channel. *Nature* 368:255–257.
20. Gähwiler BH, Brown DA (1985) GABAB-receptor-activated K+ current in voltage-clamped CA3 pyramidal cells in hippocampal cultures. *Proc Natl Acad Sci USA* 82: 1558–1562.
21. Lacey MG, Mercuri NB, North RA (1988) On the potassium conductance increase activated by GABAB and dopamine D2 receptors in rat substantia nigra neurones. *J Physiol* 401:437–453.
22. Arora D, et al. (2011) Acute cocaine exposure weakens GABA(B) receptor-dependent G-protein-gated inwardly rectifying K+ signaling in dopamine neurons of the ventral tegmental area. *J Neurosci* 31:12251–12257.
23. Padgett CL, et al. (2012) Methamphetamine-evoked depression of GABA(B) receptor signaling in GABA neurons of the VTA. *Neuron* 73:978–989.
24. Sharpe AL, Varela E, Bettinger L, Beckstead MJ (2014) Methamphetamine self-administration in mice decreases GIRK channel-mediated currents in midbrain dopamine neurons. *Int J Neuropsychopharmacol* 18:pyu073.
25. Munoz MB, et al. (2016) A role for the GIRK3 subunit in methamphetamine-induced attenuation of GABAB receptor-activated GIRK currents in VTA dopamine neurons. *J Neurosci* 36:3106–3114.
26. McCall NM, et al. (2017) Selective ablation of GIRK channels in dopamine neurons alters behavioral effects of cocaine in mice. *Neuropsychopharmacology* 42:707–715.
27. Luján R, Aguado C (2015) Localization and targeting of GIRK channels in mammalian central neurons. *Int Rev Neurobiol* 123:161–200.
28. Lunn ML, et al. (2007) A unique sorting nexin regulates trafficking of potassium channels via a PDZ domain interaction. *Nat Neurosci* 10:1249–1259.
29. Ghai R, et al. (2011) Phox homology band 4.1/ezrin/radixin/moesin-like proteins function as molecular scaffolds that interact with cargo receptors and Ras GTPases. *Proc Natl Acad Sci USA* 108:7763–7768.
30. Kajii Y, et al. (2003) A developmentally regulated and psychostimulant-inducible novel rat gene mrt1 encoding PDZ-PX proteins isolated in the neocortex. *Mol Psychiatry* 8:434–444.
31. Munoz MB, Slesinger PA (2014) Sorting nexin 27 regulation of G protein-gated inwardly rectifying K^+ channels attenuates in vivo cocaine response. *Neuron* 82: 659–669.
32. Inanobe A, et al. (1999) Characterization of G-protein-gated K+ channels composed of Kir3.2 subunits in dopaminergic neurons of the substantia nigra. *J Neurosci* 19: 1006–1017.
33. Ungless MA, Whistler JL, Malenka RC, Bonci A (2001) Single cocaine exposure in vivo induces long-term potentiation in dopamine neurons. *Nature* 411:583–587.
34. Stuber GD, Stamatakis AM, Kantak PA (2015) Considerations when using cre-driver rodent lines for studying ventral tegmental area circuitry. *Neuron* 85:439–445.
35. Lammel S, et al. (2015) Diversity of transgenic mouse models for selective targeting of midbrain dopamine neurons. *Neuron* 85:429–438.
36. Gong S, et al. (2003) A gene expression atlas of the central nervous system based on bacterial artificial chromosomes. *Nature* 425:917–925.
37. Gong S, et al. (2007) Targeting Cre recombinase to specific neuron populations with bacterial artificial chromosome constructs. *J Neurosci* 27:9817–9823.
38. Robinson TE, Berridge KC (2008) Review. The incentive sensitization theory of addiction: Some current issues. *Philos Trans R Soc Lond B Biol Sci* 363:3137–3146.
39. Cates HM, et al. (2014) Threonine 149 phosphorylation enhances ΔFosB transcriptional activity to control psychomotor responses to cocaine. *J Neurosci* 34: 11461–11469.
40. Steinberg F, et al. (2013) A global analysis of SNX27-retromer assembly and cargo specificity reveals a function in glucose and metal ion transport. *Nat Cell Biol* 15: 461–471.
41. Cullen PJ (2008) Endosomal sorting and signalling: An emerging role for sorting nexins. *Nat Rev Mol Cell Biol* 9:574–582.
42. Joubert L, et al. (2004) New sorting nexin (SNX27) and NHERF specifically interact with the 5-HT4a receptor splice variant: Roles in receptor targeting. *J Cell Sci* 117: 5367–5379.
43. Nakagawa T, Asahi M (2013) β1-Adrenergic receptor recycles via a membranous organelle, recycling endosome, by binding with sorting nexin27. *J Membr Biol* 246: 571–579.
44. Lauffer BE, et al. (2010) SNX27 mediates PDZ-directed sorting from endosomes to the plasma membrane. *J Cell Biol* 190:565–574.
45. Temkin P, et al. (2011) SNX27 mediates retromer tubule entry and endosome-to-plasma membrane trafficking of signalling receptors. *Nat Cell Biol* 13:715–721.
46. Bauch C, Koliwer J, Buck F, Hönck HH, Kreienkamp HJ (2014) Subcellular sorting of the G-protein coupled mouse somatostatin receptor 5 by a network of PDZ-domain containing proteins. *PLoS One* 9:e88529.
47. Hussain NK, Diering GH, Sole J, Anggono V, Huganir RL (2014) Sorting nexin 27 regulates basal and activity-dependent trafficking of AMPARs. *Proc Natl Acad Sci USA* 111:11840–11845.
48. Loo LS, Tang N, Al-Haddawi M, Dawe GS, Hong W (2014) A role for sorting nexin 27 in AMPA receptor trafficking. *Nat Commun* 5:3176.
49. Cai L, Loo LS, Atlashkin V, Hanson BJ, Hong W (2011) Deficiency of sorting nexin 27 (SNX27) leads to growth retardation and elevated levels of N-methyl-D-aspartate receptor 2C (NR2C). *Mol Cell Biol* 31:1734–1747.
50. Wang X, et al. (2013) Loss of sorting nexin 27 contributes to excitatory synaptic dysfunction by modulating glutamate receptor recycling in Down's syndrome. *Nat Med* 19:473–480.
51. Balana B, et al. (2011) Mechanism underlying selective regulation of G protein-gated inwardly rectifying potassium channels by the psychostimulant-sensitive sorting nexin 27. *Proc Natl Acad Sci USA* 108:5831–5836.
52. Ma D, et al. (2002) Diverse trafficking patterns due to multiple traffic motifs in G protein-activated inwardly rectifying potassium channels from brain and heart. *Neuron* 33:715–729.
53. Herman MA, et al. (2015) GIRK3 gates activation of the mesolimbic dopaminergic pathway by ethanol. *Proc Natl Acad Sci USA* 112:7091–7096.
54. Kotecki L, et al. (2015) GIRK channels modulate opioid-induced motor activity in a cell type- and subunit-dependent manner. *J Neurosci* 35:7131–7142.
55. Lalive AL, et al. (2014) Firing modes of dopamine neurons drive bidirectional GIRK channel plasticity. *J Neurosci* 34:5107–5114.
56. Johnson SW, North RA (1992) Opioids excite dopamine neurons by hyperpolarization of local interneurons. *J Neurosci* 12:483–488.
57. Vezina P (1993) Amphetamine injected into the ventral tegmental area sensitizes the nucleus accumbens dopaminergic response to systemic amphetamine: An in vivo microdialysis study in the rat. *Brain Res* 605:332–337.
58. Cornish JL, Kalivas PW (2001) Repeated cocaine administration into the rat ventral tegmental area produces behavioral sensitization to a systemic cocaine challenge. *Behav Brain Res* 126:205–209.
59. Boekhoudt L, et al. (2016) Chemogenetic activation of dopamine neurons in the ventral tegmental area, but not substantia nigra, induces hyperactivity in rats. *Eur Neuropsychopharmacol* 26:1784–1793.
60. Vezina P, Stewart J (1990) Amphetamine administered to the ventral tegmental area but not to the nucleus accumbens sensitizes rats to systemic morphine: Lack of conditioned effects. *Brain Res* 516:99–106.
61. Boekhoudt L, et al. (2017) Chemogenetic activation of midbrain dopamine neurons affects attention, but not impulsivity, in the five-choice serial reaction time task in rats. *Neuropsychopharmacology* 42:1315–1325.
62. Winstanley CA, et al. (2010) Dopaminergic modulation of the orbitofrontal cortex affects attention, motivation and impulsive responding in rats performing the five-choice serial reaction time task. *Behav Brain Res* 210:263–272.
63. Rogers RD, Baunez C, Everitt BJ, Robbins TW (2001) Lesions of the medial and lateral striatum in the rat produce differential deficits in attentional performance. *Behav Neurosci* 115:799–811.
64. Economidou D, Theobald DE, Robbins TW, Everitt BJ, Dalley JW (2012) Norepinephrine and dopamine modulate impulsivity on the five-choice serial reaction time task through opponent actions in the shell and core sub-regions of the nucleus accumbens. *Neuropsychopharmacology* 37:2057–2066.
65. Hearing M, et al. (2013) Repeated cocaine weakens GABA(B)-Girk signaling in layer 5/6 pyramidal neurons in the prelimbic cortex. *Neuron* 80:159–170.
66. Edwards NJ, et al. (2017) Circuit specificity in the inhibitory architecture of the VTA regulates cocaine-induced behavior. *Nat Neurosci* 20:438–448.
67. Beckstead MJ, Grandy DK, Wickman K, Williams JT (2004) Vesicular dopamine release elicits an inhibitory postsynaptic current in midbrain dopamine neurons. *Neuron* 42: 939–946.
68. Roth RH (1984) CNS dopamine autoreceptors: Distribution, pharmacology, and function. *Ann N Y Acad Sci* 430:27–53.
69. Bello EP, et al. (2011) Cocaine supersensitivity and enhanced motivation for reward in mice lacking dopamine D2 autoreceptors. *Nat Neurosci* 14:1033–1038.
70. Calipari ES, et al. (2014) Amphetamine self-administration attenuates dopamine D2 autoreceptor function. *Neuropsychopharmacology* 39:1833–1842.
71. Damseh N, et al. (2015) A defect in the retromer accessory protein, SNX27, manifests by infantile myoclonic epilepsy and neurodegeneration. *Neurogenetics* 16:215–221.
72. Guzman SJ, Schlögl A, Schmidt-Hieber C (2014) Stimfit: Quantifying electrophysiological data with Python. *Front Neuroinform* 8:16.